Cationic Surfactant (HDTMA)-Loaded Fly Ash for Effective Removal of Benzene Derivatives from Wastewater

S. Mushtaq,[a,b] U. Aslam,[a] R. Ali,[a,b] S. Naseem,[a] M. Ashraf,[c] Z. Aslam,[a,*] and A. Tariq[a]

[a]Department of Chemical Engineering, University of Engineering and Technology, Lahore 54890, Pakistan

[b]Khalifa University, Abu Dhabi 127788, United Arab Emirates

[c]Institute of Chemical Sciences, Bahauddin Zakariya University, 60800 Multan, Pakistan

doi: https://doi.org/10.15255/CABEQ.2024.2354

Original scientific paper
Received: July 26, 2024
Accepted: January 7, 2025

In this study, the cationic surfactant hexadecyl trimethylammonium bromide (HDTMA) was loaded onto coal fly ash and subsequently utilized for wastewater treatment. The surfactant-treated ash was characterized to investigate its porosity, surface morphology, thermal stability, and the presence of surface functional groups. Experimental studies were conducted under varying solution pH, adsorbent dosage, temperature, time, and initial pollutant concentration to obtain data for isothermal, kinetic, and thermodynamic analysis. The equilibrium uptake capacities of chlorobenzene (CB) and nitrobenzene (NB) using HDTMA-modified coal fly ash (HCFA) were found to be 214 mg g^{-1} and 74 mg g^{-1}, respectively. Kinetic analysis revealed that the pseudo-second-order model accurately described the adsorption kinetics for both benzene derivatives, while isotherm model investigations demonstrated multilayer adsorption on the HCFA surface. The isotherm data of CB and NB conformed to the Koble Corrigan and Khan Isotherm models, respectively. Thermodynamics parameters such as $\Delta G°$ (Gibbs free energy), $\Delta H°$ (enthalpy), $\Delta S°$ (entropy) and ΔH_x (isosteric heat of adsorption) were also evaluated. The results indicated that the adsorption of chlorobenzene was exothermic, spontaneous, and feasible, whereas nitrobenzene exhibited endothermic behavior and followed the non-spontaneous process. Furthermore, variations in ΔH_x values indicated the heterogeneous nature of HCFA. Overall, the prepared adsorbent demonstrated good affinity for benzene derivatives and could be considered for the treatment of wastewater containing these pollutants.

Keywords

coal fly ash, hexadecyltrimethylammonium bromide (HDTMA), adsorption, wastewater treatment, chlorobenzene, nitrobenzene

Introduction

Chlorobenzene (CB) and nitrobenzene (NB) are extensively utilized in the pharmaceutical and textile industries, chemical manufacturing, petroleum refining, agrochemicals, and plastics production. These benzene derivatives serve as solvents and raw materials for other chemicals[1–3], as well as intermediates in the synthesis of various pesticides and dyes, dielectric materials, and heat exchangers[4]. The US Environmental Protection Agency (EPA), European Commission (EC), and China's Ministry of Environmental Protection (MEP) classify both CB and NB as priority pollutants due to their carcinogenic, teratogenic, and mutagenic properties[5]. Ranked 7th and 56th on the priority pollutants list, CB and NB are highly toxic organic compounds, making their removal both significant and urgent[6].

Methods for the abatement of chloro- and nitrobenzenes from aqueous streams include biodegradation, adsorption, ion exchange, oxidation, filtration, chemical precipitation, membrane separation, solvent extraction, electrolysis, and electrodialysis[7–10]. Among these, sorption onto a solid is a non-destructive technique often employed as a final step in wastewater treatment, particularly for pollutants at low concentrations[11–13]. Various materials, such as activated carbon, zeolites, biochar, fly ash, single and multi-walled carbon nanotubes, graphene, and metal-organic frameworks (MOF), have recently been developed for effective application in sorption of organic compounds from dilute solutions[14–17].

*Corresponding author Email: hmzaheer@uet.edu.pk

Liu *et al.*[18] modified biochar with $ZnCl_2/FeCl_3$ for the electrochemical degradation of nitrobenzene. Their research revealed that modification of biochar with both Fe and Zn enhanced NB adsorption compared to unmodified biochar, owing to a greater specific surface area and an increased number of surface functional groups. Using Zn/Fe-modified biochar in electrolysis at 2-11 V resulted in highly effective NB removal (> 93 %). Ren *et al.*[19] investigated commercial activated carbon for the adsorption of chlorobenzene and employed ozonation to regenerate the saturated activated carbon. Their findings revealed that the uptake capacity of commercial activated carbon increased from 80 to 215 mg g^{-1} after three consecutive cycles of adsorption and ozonation. This improvement in the uptake capacity was attributed to oxygen-containing functional groups on the commercial activated carbon surface. However, despite the increased capacity, the high initial and regeneration costs rendered the entire process economically inefficient.

While extensive studies on natural and synthetic adsorbents have been conducted over the years, the development of new, efficient, cost-effective, and recyclable adsorbents with high adsorption capacities remains a key focus in adsorption technology advancements[12]. Literature indicates that coal fly ash exhibits significant potential in wastewater treatment applications, and chemical modification of the surface of raw coal fly ash can enhance its utility by bypassing the intermediate step of converting raw ash into secondary materials.

Coal fly ash intercalated with hexadecyltrimethylammonium bromide (HDTMA) offers a simple and effective approach to enhance its sorption capacity due to the charged head functional groups present the structure of HDTMA.

However, the surface modification of ash using HDTMA for the removal of benzene derivatives has been rarely explored. In this study, coal fly ash was modified with the cationic surfactant HDTMA for potential application in wastewater treatment. The modified material was characterized to evaluate the surface changes induced by surfactant modification. Additionally, the removal of CB and NB from wastewater was investigated under varying process parameters. The experimental results demonstrated that the HDTMA-modified fly ash exhibited significantly enhanced sorption capacity compared to unmodified ash.

Materials and methods

Materials

Raw coal fly ash (CFA) was obtained from ICI Pakistan Limited and found to be stable in dilute basic/acidic atmosphere and neutral solutions. HDTMA was purchased from Sigma Aldrich, China. Analytical grade NB was purchased from Riedel-de Haën (Germany), while CB was supplied by RCI Labscan Limited (Thailand). Dilute solutions of hydrochloric acid (Sigma Aldrich, China) and sodium hydroxide (Merck, Germany) were used to adjust the initial pH of the pollutant solution.

CFA modification and adsorption experiments

Coal fly ash (CFA) was found to be stable in dilute basic, acidic, and neutral solutions, making it a suitable substrate for modification. To prepare the raw material, CFA was sieved through a Tyler standard screen of 80 mesh, and the undersized fraction was collected, washed thoroughly with distilled water to remove impurities, and dried in an oven at 378 K. The modification process involved the incorporation of hexadecyltrimethylammonium bromide (HDTMA) surfactant onto the CFA surface through a physical adsorption mechanism. A solution of HDTMA surfactant was prepared at a concentration of 55 mmol L^{-1}, and the dried CFA was added at a weight-to-volume (w:v) ratio of 2:125. This ratio ensured optimal interaction between the surfactant molecules and the CFA particles.

HDTMA molecules, as cationic surfactants, interacted with the negatively charged CFA surface through electrostatic attraction. At concentrations below the critical micelle concentration (CMC), a monolayer of surfactant molecules formed on the CFA surface. Conversely, at concentrations above the CMC, a bilayer structure formed, further enhancing the material's surface properties for adsorption applications. The CFA-HDTMA mixture was stirred at 1000 rpm using a hot plate magnetic stirrer (Wiggen Hauser, MSC digital, USA) at 323 K for 4 hours, to ensure uniform surfactant dispersion and promote efficient adsorption onto the CFA surface. After completion of the reaction, the solid residue was separated from the solution by filtration and thoroughly washed with distilled water to remove unbound or excess surfactant molecules. Finally, the filtered material was dried in a vacuum oven (DZF 6051, Chincan, China) at 333 K to obtain the modified product. The resulting material, named HDTMA-modified coal fly ash (HCFA), exhibited enhanced surface characteristics suitable for wastewater treatment applications.

HCFA was utilized for the removal of NB and CB through batch adsorption experiments. Adsorption was studied using 100-mL solutions with varying solute concentrations. The solutions were agitated until equilibration with known dosage, temperature, and pH on a water bath shaker (Model. No. SB. 08, Benchmark Scientific, USA). The samples were then filtered, and the remaining pollutant concentrations were analyzed using a UV-Vis spec-

Table 1 – *Isotherm, dynamic, and thermodynamic model equations*

Isotherm models[20–22]	**Freundlich** $q_e = K_F C_e^{1/n_F}$ q_e (mg g^{-1}), equilibrium adsorption uptake K_f (L g^{-1})$^{1/n}$, isotherm constant n_F, Freundlich parameter	**Dubinin-Radushkevich** $q_e = q_m \exp\left(-k_{DR}\varepsilon^2\right)$ $\varepsilon = RT\ln\left(1+1/C\right)$ $E_d = 1/\sqrt{2k_{DR}}$ k_{DR} (mol^2 kJ^{-2}), D-R isotherm constant ε (kJ mol^{-1}), Polanyi potential E_d (kJ mol^{-1}), mean adsorption energy q_m (mg g^{-1}), maximum adsorption uptake	**Hill isotherm** $q_e = \frac{q_s C_e^{n_H}}{K_H + C_e^{n_H}}$ K_H (mg L^{-1}), isotherm constant n_H, Hill binding interaction parameter q_s (mg g^{-1}), maximum adsorption uptake	**Koble Corrigan (KC)** $q_e = \frac{A_{KC} C_e^{n_{KC}}}{1 + B_{KC} C_e^{n_{KC}}}$ B_{KC} (mg L^{-1}) and A_{KC} (L^n mg^{1-n} g^{-1}) are Koble Corrigan isotherm constants n_{KC}, is KC exponent	**Khan isotherm** $q_e = \frac{q_m b_K C_e}{\left(1 + b_K C_e\right)^{a_K}}$ a_K, Khan model exponent b_K, Khan model constant
Kinetic models[23,24]	**Pseudo 1st order** $q_t = q_e[1 - \exp(-k_1 t)]$ q_t and q_e are the instantaneous and equilibrium uptake (mg g^{-1}) and k_1 (min^{-1}) represents the 1st order rate constant			**Pseudo 2nd order** $q_t = \frac{k_2\ t\ q_e^2}{\left(1 + k_2\ t\ q_e\right)}$ k_2 (g mg^{-1} min^{-1}), second order rate constant	
Thermo-dynamic equations[25,26]	**Van't Hoff equation** $\Delta G^o = -RT\ \ln(K)$ $\Delta G°$ (kJ mol^{-1}), standard Gibbs free energy change R (J mol^{-1} K^{-1}), gas constant T (K), absolute temperature K shows the partition coefficient of adsorbate	**Sorption distribution constant and thermodynamic relations** $K = C_{ad} / C_e$ $\ln K = -\Delta H^o / \left(RT\right) + \Delta S^o / R$ $\Delta G^o = \Delta H^o - T\Delta S^o$ C_{ad} (mg g^{-1}) and C_e (mg g^{-1}) are equilibrium concentration of adsorbate onto adsorbent and in the solution, respectively $\Delta H°$ (kJ mol^{-1}), $\Delta S°$ (kJ mol^{-1} K^{-1}) are enthalpy and entropy change, respectively		**Clausius-Clapeyron equation** $\ln C_e = -\Delta H_x / \left(RT\right) + C$ ΔH_x (kJ mol^{-1}), isosteric heat of adsorption C, integration constant	

trophotometer (SP3000, OPTIMA, Tokyo, Japan) at a wavelength of λ_{max} = 209 nm (chlorobenzene) and λ_{max} = 268 nm (nitrobenzene). Different factors, such as dosage (ranging from 0 to 50 mg), adsorption time, initial solution pH, initial pollutant concentration, and adsorption temperature were studied. After each run, the adsorption efficiency and/or uptake capacity were calculated using the following equations:

$$\%R = \frac{C_0 - C_f}{C_0} \cdot 100 \quad (1)$$

$$q_e = \frac{(C_0 - C_f)V}{W} \quad (2)$$

where C_0 (ppm) and C_f (ppm) are the initial and final concentrations of solutes, respectively, q_e (mg g^{-1}) is the uptake capacity, and V (mL) and W (mg) represent the volume of wastewater and mass of solid, respectively. The experimental data was further analyzed by employing kinetic, isotherm, and thermodynamic equations, as summarized in Table 1.

Characterization

Fourier-transform infrared spectroscopy (FTIR) analysis was conducted to identify surface functional groups of the samples using a FT-IR 4100 apparatus (JASCO, Japan). The FTIR spectra were recorded in the range of 500–4000 cm^{-1}. Thermogravimetric analysis (TGA) was conducted to investigate the thermal behavior of the samples using an SDT Q600 apparatus (TA instruments, USA). The analysis was carried out at a 10 K min^{-1} heating rate over a temperature range of 298 to 1073 K, with nitrogen as the purge gas at a flow rate of 20 mL min^{-1}. Field emission scanning electron microscopy (FESEM) analysis was performed using a MIRA3 apparatus (TESCAN, Czechia) to analyze the surface morphology of the prepared/modified fly ash.

Results and discussions

Characterization

Fourier-transform infrared spectroscopy

FTIR spectroscopy was employed to evaluate the impact of the cationic surface active agent on the raw CFA. The infrared spectra of raw CFA and HCFA are presented and compared in Fig. 1. The

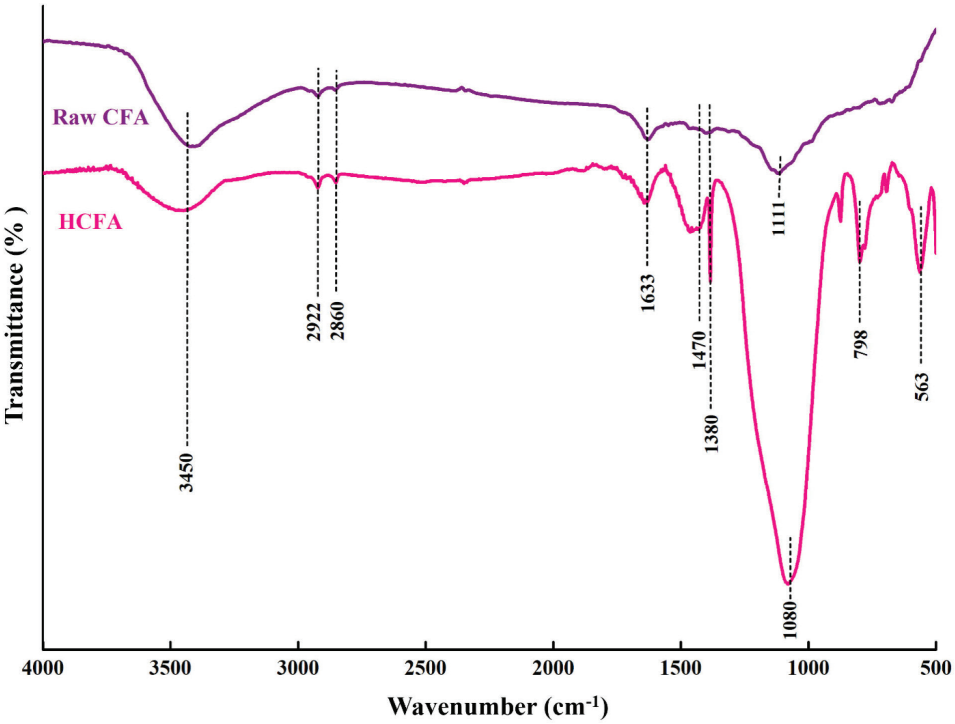

Fig. 1 – *FTIR spectrum of raw coal fly ash (CFA) and CFA modified with hexadecyl trimethylammonium bromide (HCFA)*

HCFA spectrum exhibited an IR spectrum similar to that of raw ash. The bands at approximately 3450 cm^{-1} and the peaks at about 1633 cm^{-1} correspond to O–H stretching and bending vibrations, respectively, indicating the presence of bound moisture in both fly ash samples. The transmittance peaks at 2922 and 2860 cm^{-1} represent the symmetric and asymmetric stretching vibrations of C–H in $–CH_2$ and $–CH_3$ alkyl groups, providing evidence of surfactant deposition on the fly ash surface[27–31]. Distinct new peaks between 1380 and 1470 cm^{-1} in the HCFA spectrum can be associated with the bending vibrations of CH_2, CH_3 and C–C aliphatic chains[30–34]. The peak at 1111 cm^{-1} in the raw CFA spectrum, can be attributed to the asymmetric stretching vibrations of Si–O–Al and Si–O–Si bonds. This peak intensifies and broadens after surfactant treatment of CFA, indicating the interaction of the polar active surfactant with Si–O and Al–O bonds in the fly ash. The peak value also shifts to a lower wavenumber, i.e., 1080 cm^{-1}, possibly due to the replacement of hydrogen in Si–OH with long functional groups ($Si–O[(CH_3)_3NC_{16}H_{33}]$) from the HDTMA surfactant.

Two small but sharp peaks at 798 cm^{-1} and 563 cm^{-1} correspond to the CH_2 and C–C skeletal structures present in the cationic surfactant. The presence of these peaks in the IR spectra clearly confirms the successful deposition of HDTMA on the fly ash surface.

Thermogravimetric analysis

Thermogravimetric analysis (TGA) was used to evaluate the thermal stability of the samples and to identify and compare the various stages of thermal degradation. Fig. 2 presents the changes in percent mass (TG) and derivative mass (DTG) losses for raw CFA and HCFA during heating. The thermal degradation profiles of each of the two samples can be subdivided into four stages: dehydration, devolatilization, decomposition, and char formation, as shown in Fig. 2. Stage 1 represents moisture loss, which occurred between 283 K and 373 K, and negligible mass loss was observed in either sample (maximum 2 %). Stage 2 of thermal degradation began at 373 K and extended up to 723 K, involving the removal of chemically bonded water and the devolatilization of the sample. In the DTG curve of HCFA, a small kink was observed, which can be attributed to the decomposition of HDTMA, further confirming its deposition on the fly ash[35]. Stage 3 was represented by a significant mass loss up to 973 K (decomposition). Mass losses of approximately 10 % and 8 % were recorded for raw CFA and HCFA from ~723 to 1023 K, respectively, due to the residual coal decomposition in the fly ash. The central peak in the derivative TG profile represents this decomposition stage, with peak temperatures at 883 K for raw CFA and 981 K for HCFA. The shift of the peak temperature to a higher value in HCFA suggests enhanced thermal stability, likely due to

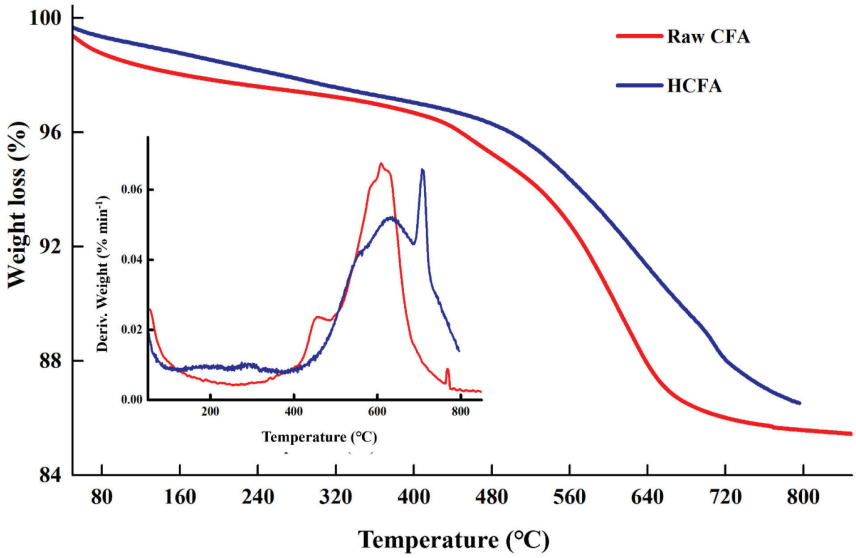

Fig. 2 – *Thermogravimetric analysis of raw coal fly ash (CFA) and CFA modified with hexadecyl trimethylammonium bromide (HCFA)*

the strong linking and electrostatic interactions between the silica and zeolitic material present in the coal fly ash and the HDTMA[36,37].

Stage 4 was the tailing stage that began at 973 K. Unlike raw CFA, HCFA exhibited a higher final residue, indicating the presence of non-volatile intercalated char resulting from the decomposition of the organic ionic chain in HCFA.

Scanning electron microscopy

The morphology of fly ash is primarily influenced by combustion process parameters such as burning temperature and ash cooling rate. To better understand the structural changes in fly ash before and after chemical treatment, SEM micrographs of RCFA and HCFA are shown in Figs. 3(a) and 3(b). In Fig. 3(a), the surface of RCFA appears rough and consists of irregularly shaped and hollow unburned carbon particles, aggregated minerals, and agglomerated particles. The surface roughness, voids, irregularity in particle shapes, and smaller agglomerated particles result from gas expulsion from the particle interior, as well as melting and fusion processes occurring during coal combustion. Generally, fly ash is a heterogeneous material and surface roughness proves its porous nature.

After treatment with the cationic surfactant, the SEM micrograph in Fig. 3(b) revealed the formation of an organic layer on the surface of CFA, resulting in increased surface smoothness. The glazed layer reduced the surface roughness, as the holes, the irregularly shaped particles, and the agglomerated and aggregated particles disappeared, indicating good interaction between HDTMA and the ash particles. After modification, the HCFA surface resembled a rocky texture with occasional cracks.

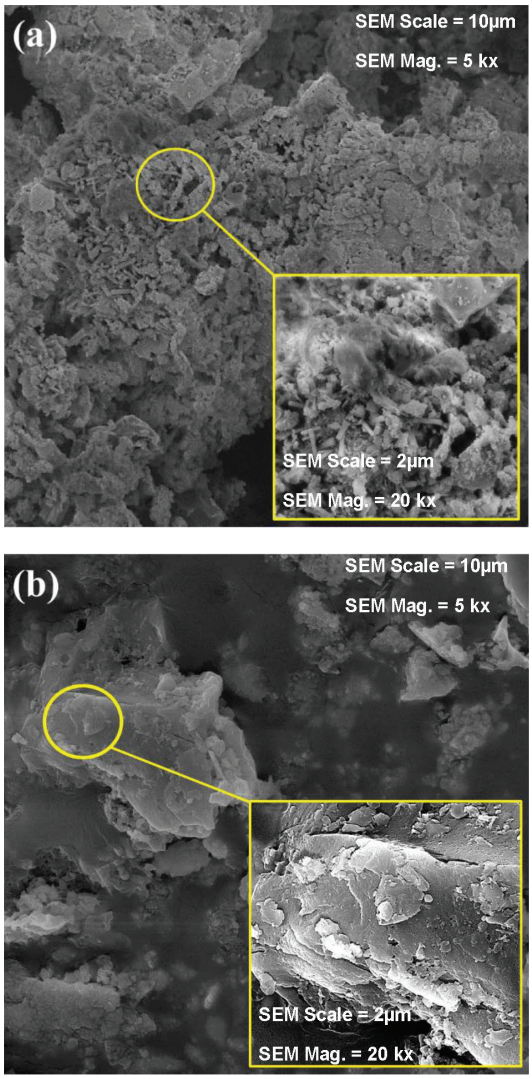

Fig. 3 – *SEM micrographs of (a) raw coal fly ash, and (b) CFA modified with hexadecyl trimethylammonium bromide*

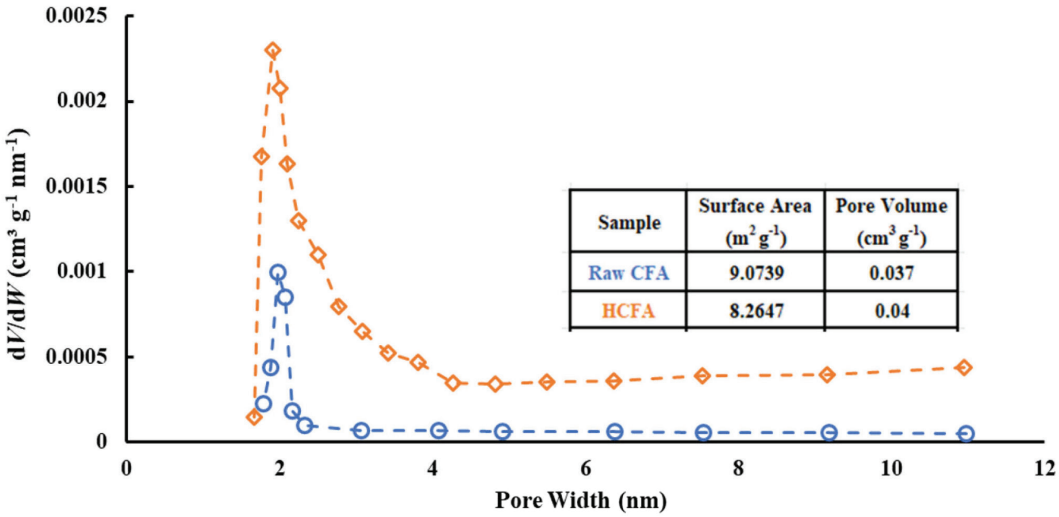

Fig. 4 – *Barrett-Joyner-Halenda pore size distribution and surface area of raw coal fly ash (CFA) and CFA modified with hexadecyl trimethylammonium bromide (HCFA)*

Pore size distribution and surface area

The Barrett-Joyner-Halenda (BJH) pore size distribution and Brunauer-Emmett-Teller (BET) surface area analyses for raw and surfactant-modified fly ash are presented in Fig. 4. The surfactant treatment significantly influenced the surface characteristics of raw fly ash. A sharp peak in the 0 – 20 nm range indicates the presence of micro- and mesopores on both the raw and modified surfaces. Beyond this range, the peak sharpness gradually decreased up to 120 nm, indicating a smaller amount of macropores. However, the narrower peak of the raw fly ash indicates that the pores were much less developed than in HCFA. HCFA exhibited a lower BET surface area of 8.26 m^2 g^{-1} and a higher pore volume of 0.040 cm^3 g^{-1} compared to CFA (as shown in the inset of Fig. 4). This was likely due to the HDTMA layer covering the raw ash surface, as supported by the SEM images. The layer of HDTMA molecules on the fly ash surface impeded nitrogen molecule diffusion into some of the pores, leading to a lower adsorption capacity[38]. The formation of the HDTMA surface layer can be attributed to electrostatic interactions.

Adsorption experimental factors

Effect of adsorbent dosage and initial solution pH

The dosage of HCFA had a positive effect on the percent removal of both NB and CB, as shown in Fig. 5. Modification of CFA with surfactant enhanced the removal percentage of both pollutants. Increasing the adsorbent dosage for a fixed pollutant concentration increased the availability of adsorption sites, improving removal efficiency. For CB, in the removal efficiency improved noticeably up to 0.15 mg mL^{-1}, beyond which the increase became less significant. For NB, the removal efficiency began to plateau around 0.1 mg mL^{-1}, likely due to the saturation of available pollutant molecules at higher adsorbent doses, leaving excess adsorption sites unutilized. Further experiments and repeated measurements confirmed this trend, suggesting that equilibrium was approached rather than complete removal. The maximum removal efficiencies using HCFA were ~ 30 % for NB and ~90 % for CB. The higher removal rate of CB can be attributed to its greater electronegativity compared to NB, enhancing its attraction to the surface. Given that benzene derivatives are difficult to ionize, ion-exchange, metal anionic surface coordination, and electrostatic interactions are unlikely to be the mechanisms of adsorption. Instead, the primary mechanisms for NB and CB removal may be ion-dipole interactions, hydrophobic interactions, and hydrogen bonding[12,39]. The response of HCFA against different solution pH's helps to reveal the mechanism of adsorption. The surface response of CFA and HCFA is presented in Fig. 6. The point of zero charge — where $\Delta pH = 0$, defined as the difference between final and initial pH (pH_f and pH_i) — for both CFA and HCFA, lies between 8 and 9. At pH levels higher than the point of zero charge, the adsorbent surface had net negative charge due to deprotonation of surface hydrophilic heads. However, at pH levels below the point of zero charge, the adsorbent surface became positively charged due to the protonation of amine surface functional groups[40,41]. Further, the response of the uptake of NB and CB on pH is shown in Fig. 7.

The results indicate that the uptake of CB increased with initial solution pH, whereas NB exhibited the opposite trend. Both CB and NB tended to deactivate the aromatic ring due to their surface inductive effects. In the case of CB, the inductive ef-

fect enhanced the electrophilicity of the carbon atoms on the ring, rendering the ring highly electropositive[42]. For pH < pH_{PZC}, the positively charged HCFA surface attracted the predominantly electronegative chlorine atom ($–Cl^{–\delta}$). Increasing solution pH enhanced the adsorption of chlorobenzene (CB) from 200 mg g^{-1} to 240 mg g^{-1}, up to the point of zero charge (PZC), as shown in Fig. 6. However, even beyond the PZC, the CB adsorption rate increased further to 250 mg g^{-1}, due to the attraction between the highly electropositive carbon ring in CB and the negatively charged HCFA sur-

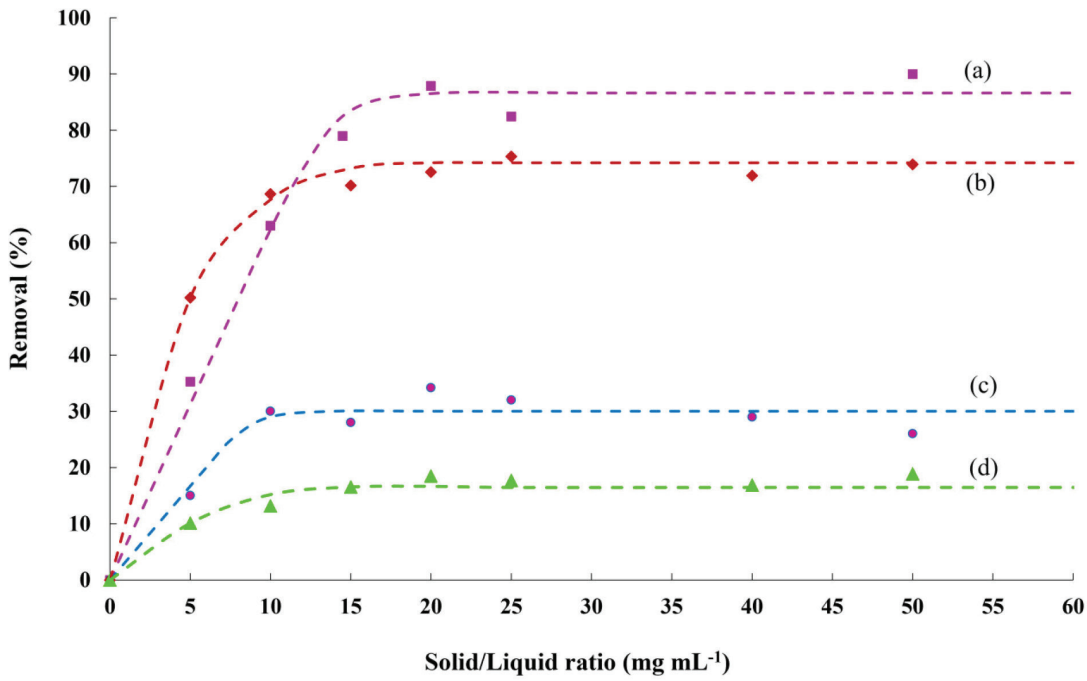

Fig. 5 – *Effect of adsorbent dose on chlorobenzene removal with (a) coal fly ash modified with hexadecyl trimethylammonium bromide (HCFA) and (b) raw CFA, and nitrobenzene removal using (c) HCFA and (d) raw CFA [fixed conditions: temperature of 30±1 °C, pollutant concentration of 50 ppm, 100 mL of solution, adsorption time of 1 h] The symbols in the plot show the experimental points, whereas dashed lines are the trend lines.*

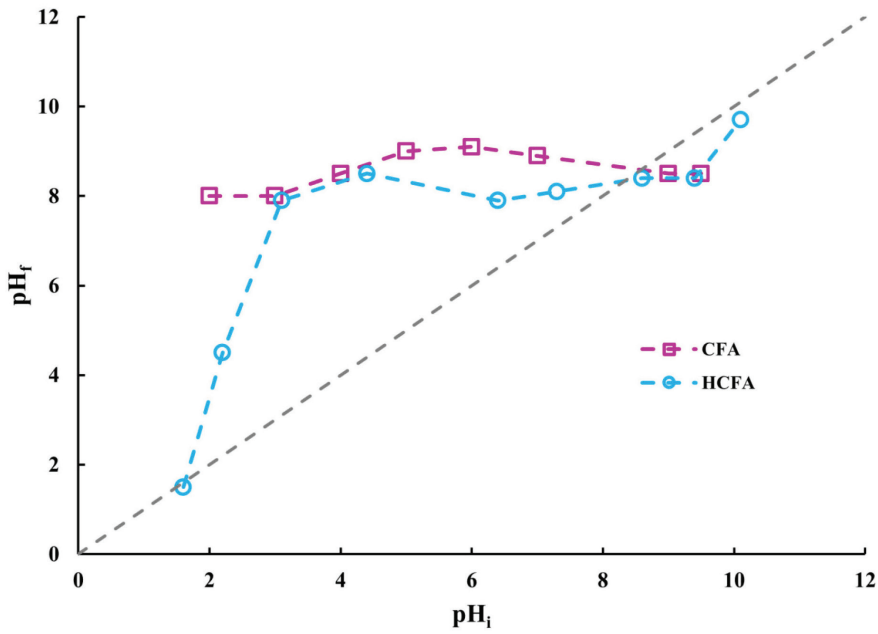

Fig. 6 – *Comparison of final and initial pH (pH_f and pH_i, respectively). The intersection of the curve and diagonal indicates the point of zero charge (PZC) of (a) raw coal fly ash (CFA) and (b) CFA modified with hexadecyl trimethylammonium bromide (HCFA).*

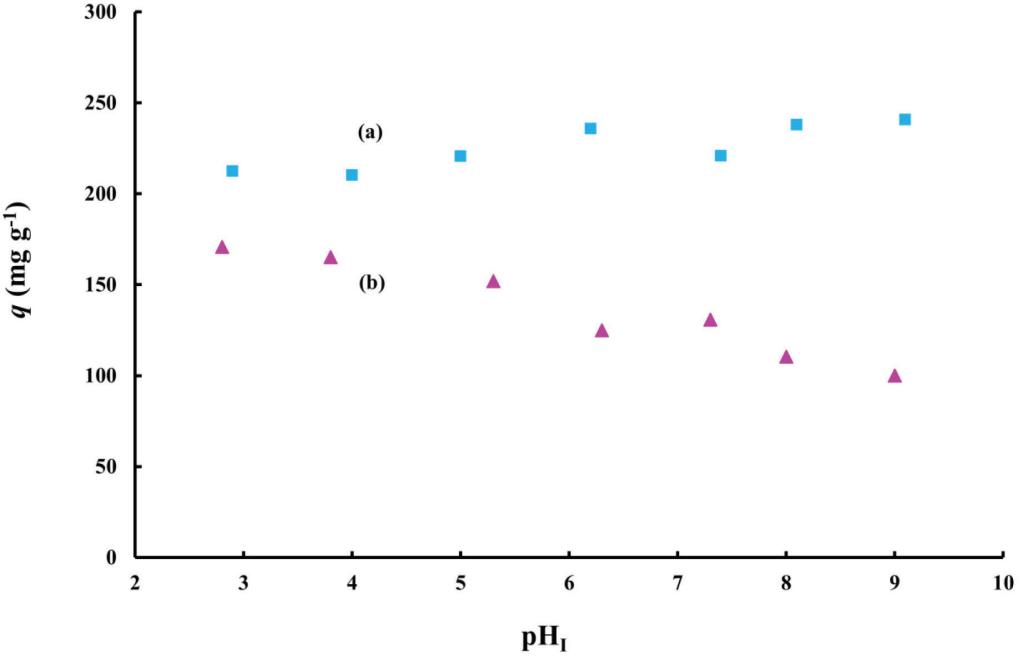

Fig. 7 – *Effect of initial solution pH (pH_I) on sorption capacity (q) of (a) chlorobenzene and (b) nitrobenzene on coal fly ash modified with hexadecyl trimethylammonium bromide [fixed conditions: pollutant concentration of 50 ppm, 100 mL of solution, dosage of 0.2 mg mL^{-1}, adsorption time of 1 h, temperature of 30±1 °C]*

face. In contrast, the adsorption of nitrobenzene (NB) gradually decreased as the surface positivity decreased. In NB, oxygen is more electronegative than nitrogen and the ring, and the oxygen acts as a dominating nucleophilic atom, attracting the positive ions[43]. This would suggest that the nucleophilic oxygen ($^{-\delta}O{=}N^{+}{-}O^{-}$) in NB, which has a strong affinity for the adsorbent surface due to a strong electrostatic attraction, is less effective at higher pH levels. As the pH increased, the positive charge on the HCFA surface diminished and eventually became completely negative after the point of zero charge (PZC). This reduction in positive charge led to decreased uptake of nitrobenzene (NB) due to the repulsion between the nitro group's nucleophilic oxygen atom ($^{-\delta}O{=}N^{+}{-}O^{-}$) and the negatively charged adsorbent surface[43]. Additionally, the overall adsorption of chlorobenzene (CB) was higher than that of NB. This is because CB has a stronger inductive effect, which enhances its susceptibility to electrophilic attack compared to nitrobenzene[44].

Adsorption kinetics

Uptake of both CB and NB increased with adsorption time, eventually leveling off at 214 mg g^{-1} and 74 mg g^{-1}, respectively, as shown in Fig. 8. The initial response of CB is steeper than that of NB due to its higher sorption affinity. Overall, the data suggest that 30 minutes is sufficient to achieve the sorption equilibrium under the experimental conditions. The contact time data were analyzed using pseudo-first-order and pseudo-second-order kinetic models via non-linear regression. The corresponding equations for each model are provided in Table 1. To evaluate the goodness of fit, the regression coefficients (R^2) and residual sum of squares (RSS) were compared for each model in Table 2. The results indicate that the pseudo-second-order model provided a better fit, demonstrated by higher R^2 values and lower RSS compared to the pseudo-first-order model. Additionally, the minimal difference between the experimental and calculated uptake capacities further supported the accuracy of the pseudo-second-order model.

Table 2 – *Regression results obtained from modeling of experimental adsorption data*

Kinetic model	Model parameter	Chlorobenzene	Nitrobenzene
Pseudo 1st Order	k_1 (min^{-1})	1.106	0.645
	$q_{e,cal}$ (mg g^{-1})	210.8	71.2
	$q_{e,exp}$ (mg g^{-1})	214	74
	R^2	0.92202	0.92636
	RSS*	284.324	70.482
Pseudo 2nd Order	$q_{e,cal}$ (mg g^{-1})	218.1	74.1
	k_2 (g min^{-1} mg^{-1})	0.0097	0.016
	R^2	0.98786	0.98587
	RSS*	44.271	13.524

*RSS stands for residual sum of squares

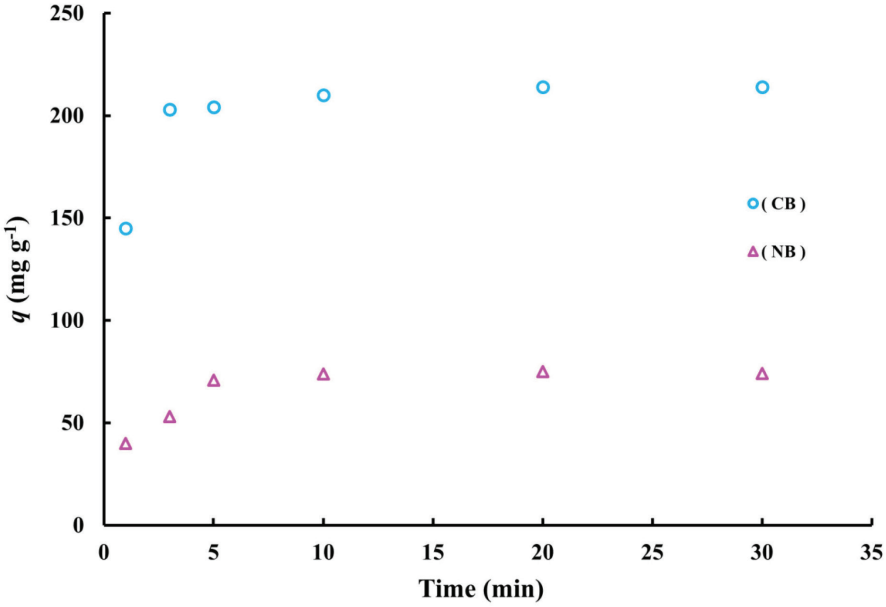

Fig. 8 – *Adsorption kinetics of chlorobenzene (CB) and nitrobenzene (NB) onto coal fly ash modified with hexadecyl trimethylammonium bromide [fixed conditions: 100 mL solution, pollutant concentration of 50 ppm, adsorbent dose of 0.2 mg mL^{-1}, temperature of 30±1 °C]*

Table 3 – *Nonlinear regression results of different isotherm models for chlorobenzene and nitrobenzene adsorption onto coal fly ash modified with hexadecyl trimethylammonium bromide at different temperatures [fixed conditions: 100 mL solution volume, adsorbent dose of 0.2 mg mL^{-1}]*

Isotherm model	Parameter	Chlorobenzene Temperature (K)				Nitrobenzene Temperature (K)			
		293	303	313	323	293	303	313	323
Freundlich	K_F	0.208	0.048	0.033	0.0042	$7.13\cdot10^{-7}$	$9.42\cdot10^{-4}$	0.00812	0.0723
	n_F	0.393	0.343	0.336	0.286	0.248	0.372	0.438	0.535
	R^2	0.983	0.985	0.991	0.985	0.987	0.996	0.978	0.972
Dubinin-Radushkevich (D-R)	q_m	11853	10935	8767	12122	6789	4422	2347	2104
	K_{DR}	$2.445\cdot10^{-4}$	$2.771\cdot10^{-4}$	$3.04\cdot10^{-4}$	$4.00\cdot10^{-4}$	0.009	0.006	0.003	0.002
	E_d	0.045	0.042	0.040	0.035	0.007	0.008	0.012	0.013
	R^2	0.965	0.979	0.983	0.972	0.978	0.973	0.968	0.918
Hill	Qs	$2.31\cdot10^{7}$	$2.045\cdot10^{6}$	$1.635\cdot10^{6}$	$1.26\cdot10^{6}$	$4.7\cdot10^{7}$	$1.52\cdot10^{6}$	$1.54\cdot10^{6}$	$6.28\cdot10^{6}$
	K_H	1441	408	386	263	1508	1024	1974	5831
	n_H	2.546	2.921	2.978	3.503	4.978	4.032	2.912	2.398
	R^2	0.980	0.981	0.985	0.977	0.991	0.986	0.994	0.972
Koble Corrigan	A_{KC}	1.634	4.508	7.097	4.715	1.657	3.40	5.589	9.634
	B_{KC}	$-6.4\cdot10^{-4}$	–0.00516	–0.0117	–0.0090	–0.0153	–0.0174	–0.0266	–0.0401
	n_{KC}	1.823	1.356	1.139	1.207	0.784	0.752	0.672	0.591
	R^2	0.979	0.978	0.978	0.968	0.997	0.99	0.998	0.993
Khan	q_m	1343	469	135	114	631	3513	10122	23440
	b_K	0.0049	0.0079	0.0181	0.0123	$2.043\cdot10^{-4}$	$1.791\cdot10^{-4}$	$1.031\cdot10^{-4}$	$7.589\cdot10^{-5}$
	a_K	–13.12	–10.209	–5.503	–8.571	–102.19	–72.498	–101.83	–101.58
	R^2	0.982	0.983	0.989	0.981	0.993	0.999	0.989	0.982

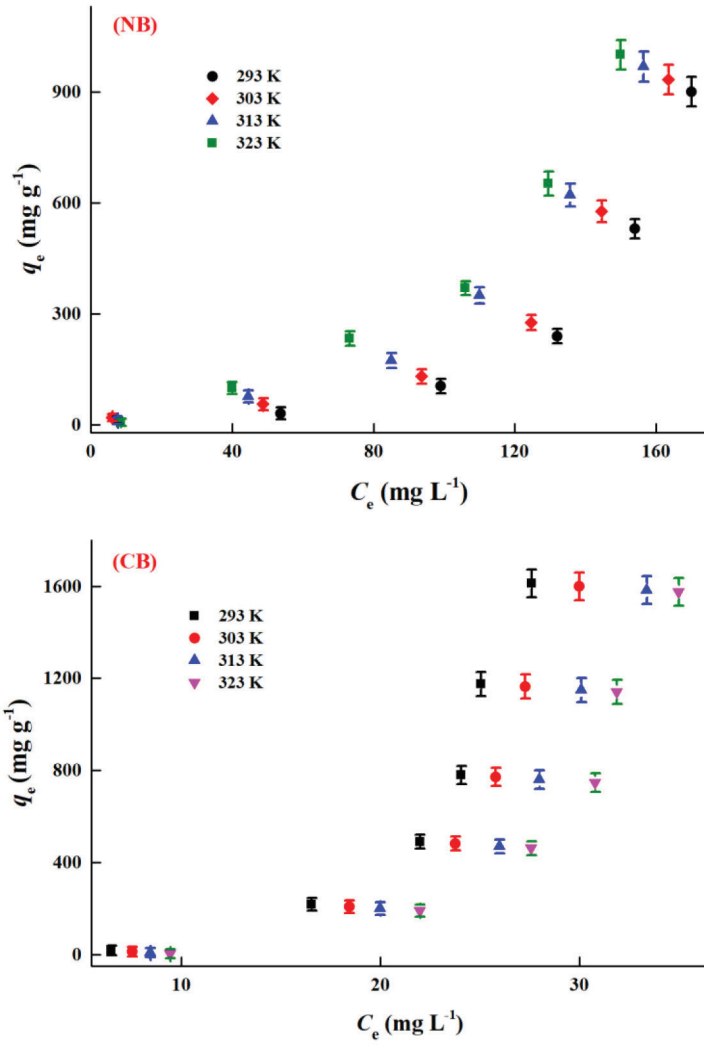

Fig. 9 – *Isotherms of nitrobenzene (NB) and chlorobenzene (CB) adsorption onto coal fly ash modified with hexadecyl trimethylammonium bromide at various temperatures [fixed conditions: 100 mL solution volume, adsorbent dose of 0.2 mg mL^{-1} dose, equilibrium sorption time]*

The rapid initial uptake characteristic of the pseudo-second-order kinetic model suggested that pore diffusion was not the rate-limiting step. This behavior indicated that the surface interactions were the primary mechanism controlling the removal of pollutants.

Adsorption isotherms

Adsorption isotherm modeling is essential for understanding the equilibrium relationship between CB and NB with HCFA. This information is crucial for optimizing and designing effluent treatment systems. Fig. 9 shows the isotherm data for CB and NB adsorption onto HCFA. Both pollutants exhibited a type III isotherm, which corresponds to the multilayer adsorption phenomenon. The uptake of chlorobenzene decreased with increasing temperature indicating an exothermic process. However, NB exhibited opposite behavior to CB, with its adsorption being endothermic in nature.

Five different models were used to analyze the adsorption mechanism. The equations for these models, along with relevant variables, are provided in Table 3. Both the Freundlich and Dubinin-Radushkevich (DR) isotherm models assume heterogeneous surfaces for the adsorbents, while the Hill model considers a homogeneous surface and determines cooperative or non-cooperative adsorption through the n_H parameter. The Koble-Corrigan and Khan models are three-parameter models, which incorporate features of both the Langmuir and Freundlich isotherms. Non-linear regression results are summarized in Table 3. The Freundlich model provided a reasonable fit to the data points, with R^2 values greater than 0.97 for chlorobenzene (CB). The Freundlich constant K_F decreased from 0.208 to 0.004 as the temperature decreased from 323 K to 293 K, confirming the exothermic nature of CB adsorption. For nitrobenzene (NB), K_F increased with rising temperature, suggesting endothermic adsorption. The mean free energy (E_d) derived from the DR isotherm was less than 16 kJ mol^{-1} for both CB and NB at all temperatures, indicating a physisorption mechanism. The n_H parameter from the Hill isotherm model was greater than 1 for both CB and NB, indicating positive cooperative binding. The q_e value from the Hill model was too high, rendering it unsuitable for describing the mechanism of pollutant adsorption onto HCFA. The Koble Corrigan model showed a fairly good correlation coefficient for CB adsorption at all temperatures, with corresponding exponent $n_{KC} > 1$, confirming the applicability of this isotherm. However, n_{KC} values were found to be < 1 for NB, making this model unsuitable for describing NB adsorption. The Khan isotherm provided high R^2 values, and was therefore well-suited to describe the NB adsorption onto HCFA.

Adsorption thermodynamics

Thermodynamic analysis revealed that CB adsorption onto HCFA was exothermic, while NB adsorption showed endothermic behavior. These characteristics were confirmed by the Van't Hoff plot presented in Fig. 10. Thermodynamic functions calculated from the linear plots are summarized in Table 4. The exothermic character of CB adsorption was evident from the negative enthalpy of adsorption ($\Delta H°$) values, which varied from minimum –16.98 kJ mol^{-1} to –4.56 kJ mol^{-1}, as shown in Table 4.

Conversely, the positive $\Delta H°$ values for NB adsorption onto HCFA indicated an endothermic process. The magnitude of $\Delta H°$ for both CB and NB

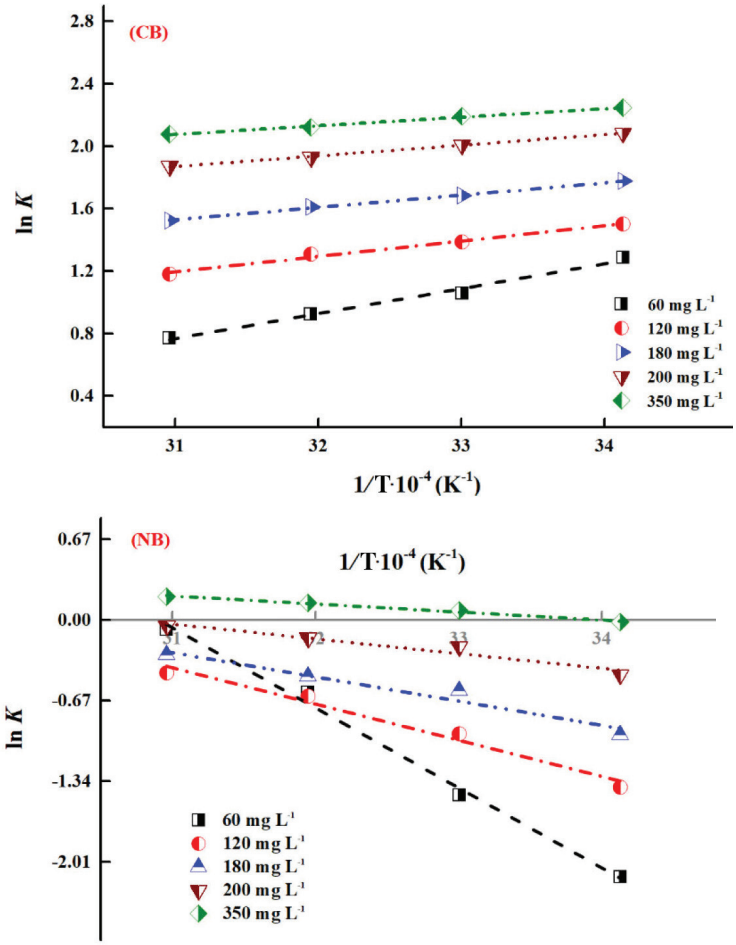

Fig. 10 – *Plots of ln K vs. 1/T (K^{-1}) for the adsorption of chlorobenzene (CB) and nitrobenzene (NB) onto coal fly ash modified with hexadecyl trimethylammonium bromide [fixed conditions: 100 mL solution volume, adsorbent dose of 0.2 mg mL^{-1}]. Legends indicate the experimental points, and discontinuous lines are the regression lines determined through excel built-in function.*

was less than 80 kJ mol^{-1}, suggesting a physical adsorption mechanism involving van der Waals forces and electrostatic interactions in the adsorption process[45,46]. The Gibbs energy ($\Delta G°$) values for CB were negative at all temperatures, indicating a spontaneous and favorable adsorption process. The decrease in the negativity of $\Delta G°$ with increasing temperature suggested that CB adsorption was thermodynamically more favorable at lower temperatures. In contrast, the positive $\Delta G°$ values for NB adsorption indicated a non-spontaneous process that required net energy input[47]. The magnitude of $\Delta G°$ decreasing with rising temperature, as shown in Table 4, indicated that higher temperatures facilitated NB adsorption. Additionally, $\Delta S°$ for CB removal indicated that the adsorption was enthalpy-driven, without significant structural changes occurring during adsorption. This reflected less disorder at the interface, possibly due to multilayer adsorption. Conversely, the positive $\Delta S°$ for NB adsorption onto HCFA suggested increased randomness at the solid/liquid interface during the adsorption process[48].

The isosteric heat of adsorption (ΔH_x) was determined using the Clausius/Clapeyron equation given in Table 1. The isosteres obtained from the plot of $\ln C_e$ vs $1/T$ corresponding to different surface coverage of CB and NB are presented in Fig. 11. The linear regression of experimental data yielded ΔH_x, summarized in Table 5, along with the corresponding correlation coefficients. Isosteric heats were found to be less than 80 kJ mol^{-1}, confirming the physisorption mechanism. The variation in ΔH_x suggested a heterogeneous HCFA surface. At higher surface coverages, ΔH_x decreased, likely due to the

Table 4 – *Thermodynamic parameters for benzene derivatives adsorption onto coal fly ash modified with hexadecyl trimethylammonium bromide*

Initial dye concentration (mg L^{-1})	Chlorobenzene					
	$\Delta H°$ (kJ mol^{-1})	$\Delta S°$ (kJ mol^{-1} K^{-1})	$\Delta G°$ (kJ mol^{-1})			
			323 K	313 K	303 K	293 K
60	–16.98	–0.047	–1.71	–2.64	–3.11	–3.58
120	–7.73	–0.014	–3.21	–3.49	–3.63	–3.76
180	–6.54	–0.008	–4.08	–4.23	–4.31	–4.38
260	–5.91	–0.003	–4.99	–5.05	–5.08	–5.11
350	–4.56	0.0031	–5.58	–5.51	–5.48	–5.45
	Nitrobenzene					
60	55.35	0.171	0.11	1.81	3.52	5.24
120	25.03	0.074	1.04	1.78	2.52	3.26
180	16.73	0.050	0.71	1.21	1.71	2.19
260	10.22	0.031	0.08	0.38	0.71	1.02
350	5.54	0.019	–0.55	–0.35	–0.17	0.02

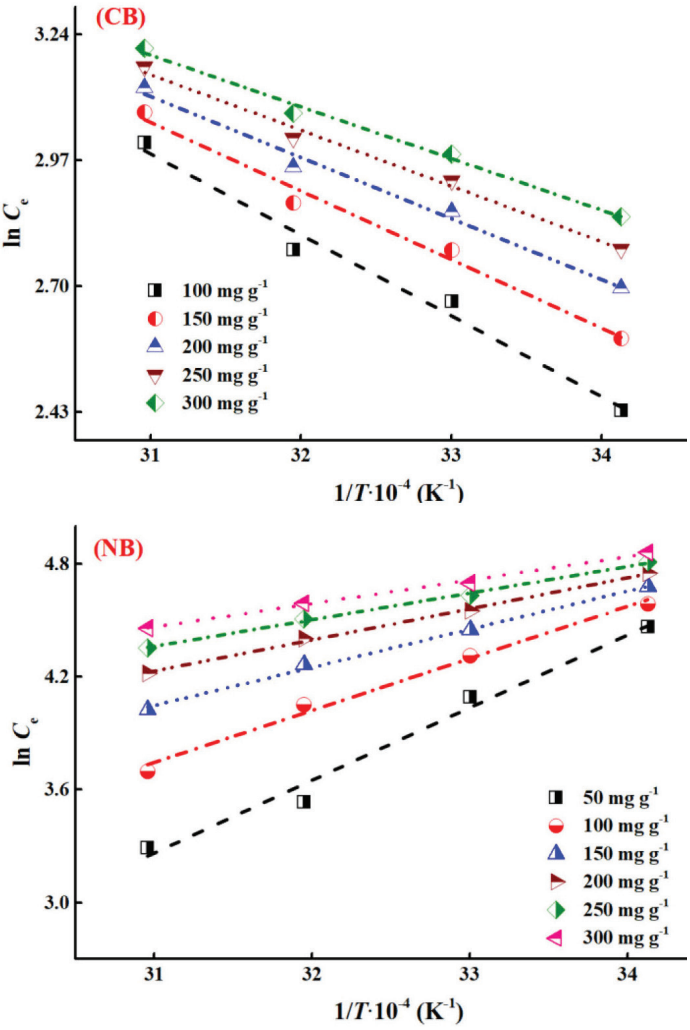

Fig. 11 – *Isosteric plots of ln C_e as a function of 1/T (K^{-1}) for chlorobenzene (CB) and nitrobenzene (NB) adsorption onto coal fly ash modified with hexadecyl trimethylammonium bromide at constant adsorbed amount [fixed conditions: 100 mL solution volume, adsorbent dose of 0.2 mg mL^{-1}]. Legends indicate the experimental points, and discontinuous lines are the regression lines determined through excel built-in function.*

Table 5 – *Isosteric heat of adsorption for chlorobenzene (CB) and nitrobenzene (NB) onto coal fly ash modified with hexadecyl trimethylammonium bromide (HCFA)*

q_e (mg g^{-1})	CB-HCFA		NB-HCFA	
	ΔH_x (kJ mol^{-1})	R^2	ΔH_x (kJ mol^{-1})	R^2
100	–14.43	0.9820	22.92	0.9907
150	–12.23	0.9855	16.84	0.9966
200	–10.88	0.9881	13.73	0.9974
250	–9.93	0.9901	11.75	0.9970
300	–9.22	0.9919	10.34	0.9960

coverage of high energy active sites during the initial stage of adsorption, followed by intermolecular interactions among adsorbed moieties, reducing the isosteric heat[49,50]. Table 6 compares the performance of biochar, cellulosic aerogels, hydroxyapatite gelatin, magnetic porous carbon, modified microporous silica material, HDTMA bentonite, high silica zeolites, carbonized sugarcane bagasse, modified magnetic diatomite, modified fly ash sieves, hydrophobic cotton fiber and graphitic nanoribbons, for the removal of CB and NB. Adsorption performance varies based on the initial pollutant concentration, adsorbent surface properties, and other adsorption process conditions. This comparison indicates that HCFA is a promising adsorbent for removing chlorobenzene and nitrobenzene from aqueous solutions.

Conclusion

The surface of coal fly ash was successfully modified through anionic surfactant hexadecyltrimethylammonium bromide (HDTMA) treatment under various experimental conditions. The resulting HCFA material was compared to untreated fly ash. The HCFA was evaluated for its effectiveness in removing organic pollutants, specifically chlorobenzene (CB) and nitrobenzene (NB), from wastewater. FTIR analysis confirmed the presence of amino and alkyl functional groups on the HCFA surface, while SEM micrographs revealed changes in surface structure due to the introduction of the cationic polymer, including the formation of an adhesive organic layer on the porous ash surface, enhancing its adsorption capacity. Thermogravimetric and BET analyses indicated that HDTMA formed strong bonds with alumina and silica, reducing thermal decomposition compared to raw ash and promoting the formation of an active adsorption layer. Batch adsorption experiments identified an optimal solid-to-liquid ratio of 0.2 mg L^{-1} for both raw CFA and HCFA, corresponding to the maximum removal of NB and CB under specific solution pH conditions. HCFA achieved maximum removal rates of 80 % for CB and 30 % for NB. The adsorption of NB and CB followed a pseudo–second-order kinetic model, suggesting that surface reactions were the primary controlling mechanism. Isotherm studies revealed that the adsorption of both pollutants followed a type III isotherm, indicating a multilayer adsorption phenomenon. The Koble Corrigan and Khan isotherm models provided the best fits for the experimental equilibrium data for CB and NB, respectively. Thermodynamic analysis revealed that CB adsorption on HCFA is spontaneous and feasible ($\Delta G°< 0$), whereas NB adsorption is non-spontaneous ($\Delta G°>0$). The negative $\Delta S°$ for CB removal suggested an enthalpy-driven adsorption process with minimal structural changes, while the positive $\Delta S°$ for NB indicated increased randomness at the solid/liquid interface. The evaluation of the isosteric heat of adsorption confirmed that HCFA possesses an energetically heterogeneous surface.

Table 6 – *Comparison of adsorption capacity of coal fly ash modified with hexadecyl trimethylammonium bromide (HCFA) with other reported adsorbents*

Adsorbent	Experimental conditions	Adsorption capacity (mg g^{-1})		Reference
		Chlorobenzene	Nitrobenzene	
Biochar (BC) and magnetic biochar (MBC)	pH: 7, time: 5 min, *T*: 298 K, nitrobenzene: (0–700 ppm), adsorbent: 2 g L^{-1}	–	193 (BC) and 178 (MBC)	[51]
Cellulose laurate ester (CE) aerogels	Time: 180 min, *T*: 298 K, chlorobenzene: (3 mmol L^{-1}), adsorbent: 0.05 g L^{-1}	2068.85	–	[52]
Hydroxyapatite-gelatin (HAP-GEL) nanocomposite	pH: 4, time: 1 h, *T*: 298 K, nitrobenzene: (2–10 ppm), adsorbent: 5 g L^{-1}	–	42.373	[53]
Hexadecyl trimethylammonium bromide modified bentonite	Time: 120 min, *T*: 298 K, chlorobenzene (28.14 ppm), adsorbent: 80 mg L^{-1}	24.12	–	[54]
Magnetic porous carbon MPC-973	Time: 2 h, *T*: 298 K, adsorbent: 30 mg L^{-1}	–	58.2	[55]
High silica zeolites i) ZSM-5 ii) Y	pH: 7, time: 24 h, *T*: 288.3 K, adsorbent: 0.5 g L^{-1}	i) 76.6 ii) 227	–	[56]
Carbonized sugarcane bagasse (SCB)	pH: 5.8, time: 90 min, *T*: 298 K, nitrobenzene: (50–500 ppm), adsorbent: 0.3 mg/50 mL	–	38.27	[57]
Modified magnetic diatomite	*T*: 288 K, nitrobenzene (0–200 ppm), adsorbent: 0.1 mg/25 mL	–	54.31	[58]
Primary polyethylene microplastics	pH: 7.30, time: 48 h, *T*: 298 K, chlorobenzene: (0–0.1 ppm), adsorbent: 10 mg/30 mL	0.227	–	[59]
Fly ash derived mesoporous silica SBA-15	pH: 5, Time: 60 min, *T*: 298 K, nitrobenzene: 8 μmol L^{-1}, adsorbent: 5.5 g L^{-1}	–	6.39	[60]
Hydrophobic cotton fibers (HCF)	pH: 7, Time: 2 h, *T*: 303 K, nitrobenzene: (0–2 ppm), adsorbent: 0.1 g L^{-1}	–	16.85	[61]
Hexadecyl trimethylammonium bromide modified coal fly ash	Time: 1 h, *T*: 303 K, nitrobenzene: 50 ppm, chlorobenzene: 50 ppm, adsorbent: 0.2 mg mL^{-1}	214	74	this study

ACKNOWLEDGMENTS

The authors gratefully acknowledge the support of the Higher Education Commission, Pakistan, through the National Research Program for Universities for funding this research under project 8039/Punjab/NRPU/R&D/HEC/2017. They also extend their gratitude to the Department of Chemical Engineering, UET, Lahore, for their support.

DATA AVAILABILITY STATEMENT

The authors confirm that the data supporting the findings of this study are available within the article.

COMPLIANCE WITH ETHICAL STANDARDS

The authors declare that they have no conflict of interest.

References

1. *Zhao, X., Zeng, X., Qin, Y., Li, X., Zhu, T., Tang, X.,* An experimental and theoretical study of the adsorption removal of toluene and chlorobenzene on coconut shell derived carbon, Chemosphere **206** (2018) 285. doi: https://doi.org/10.1016/j.chemosphere.2018.04.126
2. *Sennour, R., Mimane, G., Benghalem, A., Taleb, S.*, Removal of the persistent pollutant chlorobenzene by adsorption onto activated montmorillonite, Appl. Clay Sci. **43** (2009) 503. doi: https://doi.org/10.1016/j.clay.2008.06.019
3. *Jose, J., Philip, L.*, Degradation of chlorobenzene in aqueous solution by pulsed power plasma: Mechanism and effect of operational parameters, J. Environ. Chem. Eng. **7** (2019) 103476. doi: https://doi.org/10.1016/j.jece.2019.103476
4. *Zhu, R., Mao, Y., Jiang, L., Chen, J.*, Performance of chlorobenzene removal in a nonthermal plasma catalysis reactor and evaluation of its byproducts, Chem. Eng. J. **279** (2015) 463. doi: https://doi.org/10.1016/j.cej.2015.05.043
5. *Mu, M., Zhang, X., Yu, G., Sun, C., Xu, R., Liu, N., Wang, N., Chen, B., Dai, C.*, Deep removal of chlorobenzene based volatile organic compounds from exhaust gas with ionic liquids, Sep. Purif. Technol. **298** (2022) 121610. doi: https://doi.org/10.1016/j.seppur.2022.121610
6. https://www.epa.gov/sites/production/files/2015-09/documents/priority-pollutant-list-epa.pdf 2014
7. *Mohan, A., Nimisha, K. V. N., Janardanan, C.,* Removal of chlorobenzene and 1,4-dichlorobenzene using novel poly-*o*-toluidine zirconium(IV) phosphotellurite exchanger, Resour. Technol. **3** (2017) 317. doi: https://doi.org/10.1016/j.reffit.2017.02.003
8. *Pandey, R. A., Joshi, P. R., Mudliar, S. N., Deshmukh, S. C.,* Biological treatment of waste gas containing mixture of monochlorobenzene (MCB) and benzene in a bench scale biofilter, Bioresour. Technol. **101** (2010) 5168. doi: https://doi.org/10.1016/j.biortech.2010.02.017
9. *Li, F., Chen, C., Wang, Y., Li, W., Zhou, G., Zhang, H., Zhang, J., Wang, J.,* Activated carbon-hybridized and amine-modified polyacrylonitrile nanofibers toward ultra-high and recyclable metal ion and dye adsorption from wastewater, Front. Chem. Sci. Eng. **15** (2021) 984. doi: https://doi.org/10.1007/s11705-020-2000-3
10. *Jiang, F., Li, Y., Zhou, W., Yang, Z., Ning, Y., Liu, D., Tang, Z., Yang, S., Huang, H., Wang, G.,* Enhanced degradation of monochlorobenzene in groundwater by ferrous iron/persulfate process with cysteine, Chem. Eng. J. **387** (2020) 124048. doi: https://doi.org/10.1016/j.cej.2020.124048
11. *Tan, X. F., Zhu, S. S., Wang, R. P., Chen, Y. Di., Show, P. L., Zhang, F. F., Ho, S. H.,* Role of biochar surface characteristics in the adsorption of aromatic compounds: Pore structure and functional groups, Chin. Chem. Lett. **32** (2021) 2939 doi: https://doi.org/10.1016/j.cclet.2021.04.059
12. *Wei, W., Sun, R., Cui, J., Wei, Z.,* Removal of nitrobenzene from aqueous solution by adsorption on nanocrystalline hydroxyapatite, Desalination **263** (2010) 89. doi: https://doi.org/10.1016/j.desal.2010.06.043
13. *Awad, A. M., Jalab, R., Benamor, A., Nasser, M. S., Ba-Abbad, M. M., El-Naas, M., Mohammad, A. W.,* Adsorption of organic pollutants by nanomaterial-based adsorbents: An overview, J. Mol. Liq. **301** (2020) 112335. doi: https://doi.org/10.1016/j.molliq.2019.112335
14. *Soffian, M. S., Abdul Halim, F. Z., Aziz, F. A., Rahman, M., Mohamed Amin, M. A., Awang Chee, D. N.,* Carbon-based material derived from biomass waste for wastewater treatment, Environ. Adv. **9** (2022) 100259. doi: https://doi.org/10.1016/j.envadv.2022.100259
15. *Jiang, N., Shang, R., Heijman, S. G. J., Rietveld, L. C.,* High-silica zeolites for adsorption of organic micro-pollutants in water treatment: A review, Water Research **144** (2018) 145. doi: https://doi.org/10.1016/j.watres.2018.07.017
16. *Mushtaq, F., Zahid, M., Bhatti, I. A., Nasir, S., Hussain, T.,* Possible applications of coal fly ash in wastewater treatment, J. Environ. Manage. **240** (2019) 27. doi: https://doi.org/10.1016/j.jenvman.2019.03.054
17. *Reeve, P. J., Fallowfield, H. J.,* Natural and surfactant modified zeolites: A review of their applications for water remediation with a focus on surfactant desorption and toxicity towards microorganisms, J. Environ. Manage. **205** (2018) 253. doi: https://doi.org/10.1016/j.jenvman.2017.09.077
18. *Liu, Q., Jiang, S., Su, X., Zhang, X., Cao, W., Xu, Y.,* Role of the biochar modified with $ZnCl_2$ and $FeCl_3$ on the electrochemical degradation of nitrobenzene, Chemosphere **275** (2021) 129966. doi: https://doi.org/10.1016/j.chemosphere.2021.129966
19. *Ren, M., Wang, J., Wang, Z., Sun, S., Qiu, J., Shi, Y., Wang, Z. J., Xie, Y.,* Activated carbon adsorption coupled with ozonation regeneration for efficient removal of chlorobenzene, J. Environ. Chem. Eng. **10** (2022) 107319. doi: https://doi.org/10.1016/j.jece.2022.107319
20. *Syafiuddin, A., Salmiati, S., Jonbi, J., Fulazzaky, M. A.,* Application of the kinetic and isotherm models for better understanding of the behaviors of silver nanoparticles adsorption onto different adsorbents, J. Environ. Manage. **218** (2018) 59. doi: https://doi.org/10.1016/j.jenvman.2018.03.066
21. *Hashem, A., Taha, G. M., Fletcher, A. J., Mohamed, L. A., Samaha, S. H.,* Highly efficient adsorption of Cd(II) onto carboxylated camelthorn biomass: Applicability of three-parameter isotherm models, kinetics, and mechanism, J. Polym. Environ. **29** (2021) 1630. doi: https://doi.org/10.1007/s10924-020-01991-6
22. *Al-Ghouti, M. A., Da'ana, D. A.,* Guidelines for the use and interpretation of adsorption isotherm models: A review, J. Hazard. Mater. **393** (2020) 122383. doi: https://doi.org/10.1016/j.jhazmat.2020.122383
23. *Jasper, E. E., Ajibola, V. O., Onwuka, J. C.,* Nonlinear regression analysis of the sorption of crystal violet and methylene blue from aqueous solutions onto an agro-waste derived activated carbon, Appl. Water Sci. **10** (2020) 1. doi: https://doi.org/10.1007/s13201-020-01218-y
24. *Moussout, H., Ahlafi, H., Aazza, M., Maghat, H.,* Critical of linear and nonlinear equations of pseudo-first order and pseudo-second order kinetic models, Karbala Int. J. Mod. Sci. **4** (2018) 244. doi: https://doi.org/10.1016/j.kijoms.2018.04.001
25. *Hevira, L., Zilfa. R., Ighalo, J. O., Zein, R.,* Biosorption of indigo carmine from aqueous solution by *Terminalia catappa* shell, J. Environ. Chem. Eng. **8** (2020) 104290. doi: https://doi.org/10.1016/j.jece.2020.104290
26. *Al-Kadhi, N. S.,* The kinetic and thermodynamic study of the adsorption Lissamine Green B dye by micro-particle of wild plants from aqueous solutions, Egypt. J. Aquat. Res. **45** (2019) 231. doi: https://doi.org/10.1016/j.ejar.2019.05.004

27. *Alcântara, R. R., Izidoro, J. C., Fungaro, D. A.,* Synthesis and characterization of surface modified zeolitic nanomaterial from coal fly ash, International Journal of Materials Chemistry and Physics **1** (2015) 370.
28. *Mathebula, C. L.,* Surface modification of coal fly ash by sodium lauryl sulphate. PhD Thesis. University of Pretoria (2013).
http://hdl.handle.net/2263/24889
29. *Onyango, M. S., Kittinya, J., Hadebe, N., Ojijo, V. O., Ochieng, A.,* Sorpcija melanoidina na površinski modifikovanom zeolitu, Chem. Ind. Chem. Eng. Q. **17** (2011) 385.
doi: https://doi.org/10.2298/CICEQ110125025O
30. *Banerjee, S. S., Joshi, M. V., Jayaram, R. V.,* Treatment of oil spills using organo-fly ash, Desalination **195** (2006) 32.
doi: https://doi.org/10.1016/j.desal.2005.10.038
31. *Jahangiri, K., Yousefi, N., Ghadiri, S. K., Fekri, R., Bagheri, A., Talebi, S. S.,* Enhancement adsorption of hexavalent chromium onto modified fly ash from aqueous solution; optimization; isotherm, kinetic and thermodynamic study, J. Dispers. Sci. Technol. **40** (2019) 1147.
doi: https://doi.org/10.1080/01932691.2018.1496841
32. *Gao, M., Ma, Q., Lin, Q., Chang, J., Ma, H.,* Fabrication and adsorption properties of hybrid fly ash composites, Appl. Surf. Sci. **396** (2017) 400.
doi: https://doi.org/10.1016/j.apsusc.2016.10.167
33. *Pansuk, C. A*., Comparative study of the adsorption of Acid Brown 75 and Direct Yellow 162 onto unmodified and surfactant modified granule developed from coal fly ash, IPCBEE **6** (2011) 49.
34. *Rosas-Casarez, C. A., Arredondo-Rea, S. P., Cruz-Enríquez, A., Corral-Higuera, R., Pellegrini-Cervantes, M. de J., Gómez-Soberón, J. M., Medina-Serna, T. de J.,* Influence of size reduction of fly ash particles by grinding on the chemical properties of geopolymers, Appl. Sci. **8** (2018) 365.
doi: https://doi.org/10.3390/app8030365
35. *Wu, D., Sun, Y., Wang, L., Zhang, Z., Gui, J., Ding, A.,* Modification of NaY zeolite by lanthanum and hexadecyl trimethyl ammonium bromide and its removal performance for nitrate, Water Environ. Res. **92** (2020) 987.
doi: https://doi.org/10.1002/wer.1285
36. *Nguyen, T. M. T., Do, T. P. T., Hoang, T. S., Nguyen, N. V., Pham, H. D., Nguyen, T. D., Pham, T. N. M., Le, T. S., Pham, T. D.,* Adsorption of anionic surfactants onto alumina: Characteristics, mechanisms, and application for heavy metal removal, Int. J. Polym. Sci. **2018** (2018) 1.
doi: https://doi.org/10.1155/2018/2830286
37. *Li, P., Ishiguro, M.,* Adsorption of anionic surfactant (sodium dodecyl sulfate) on silica, Soil Sci. Plant Nutr. **62** (2016) 223.
doi: https://doi.org/10.1080/00380768.2016.1191969
38. *Elsheikh, A. F., Ahmad, U. K., Ramli, Z.,* Investigations on humic acid removal from water using surfactant-modified zeolite as adsorbent in a fixed-bed reactor, Appl. Water Sci. **7** (2017) 2843.
doi: https://doi.org/10.1007/s13201-016-0521-1
39. *Qin, Q., Ma, J., Liu, K.,* Adsorption of nitrobenzene from aqueous solution by MCM-41, J. Colloid Interface Sci. **315** (2007) 80.
doi: https://doi.org/10.1016/j.jcis.2007.06.060
40. *Kosmulski, M.,* PH-dependent surface charging and points of zero charge. IV. Update and new approach, J. Colloid Interface Sci. **337** (2009) 439.
doi: https://doi.org/10.1016/j.jcis.2009.04.072
41. *Furukawa, M., Tateishi, I., Katsumata, H., Kaneco, S.,* Application of sodium dodecyl sulfate/activated carbon onto the preconcentration of cadmium ions in solid-phase extraction flow system, ChemEngineering **3** (2019) 1.
doi: https://doi.org/10.3390/chemengineering3030067
42. *Aramendía, M. A., Boráu, V., García, I. M., Jiménez, C., Marinas, A., Marinas, J. M., Urbano, F. J.,* Liquid-phase hydrodehalogenation of substituted chlorobenzenes over palladium supported catalysts, Appl. Catal. B Environ. **43** (2003) 71.
doi: https://doi.org/10.1016/S0926-3373(02)00279-5
43. *Wepster, B. M.,* Steric effects on mesomerism. XVI†). Comparative investigations involving ultra-violet absorption spectra, molecular refractions, rates of reaction, and basic strengths of aromatic amines, Recl. Trav. Chim. Pays-Bas. **76** (1957) 335.
doi: https://doi.org/10.1002/recl.19570760503
44. *Heaney, H.,* Aromatic compounds, Annu. Reports Prog. Chem. – Sect. B **67** (1970) 327.
doi: https://doi.org/10.1039/OC9706700327
45. *Dovi, E., Kani, A. N., Aryee, A. A., Jie, M., Li, J., Li, Z., Qu, L., Han, R.,* Decontamination of bisphenol A and Congo red dye from solution by using CTAB functionalised walnut shell, Environ. Sci. Pollut. Res. **28** (2021) 28732.
doi: https://doi.org/10.1007/s11356-021-12550-4
46. *Sahmoune, M. N.,* Evaluation of thermodynamic parameters for adsorption of heavy metals by green adsorbents, Environ. Chem. Lett. **17** (2019) 697.
doi: https://doi.org/10.1007/s10311-018-00819-z
47. *Ali, R. M., Hamad, H. A., Hussein, M. M., Malash, G. F.,* Potential of using green adsorbent of heavy metal removal from aqueous solutions: Adsorption kinetics, isotherm, thermodynamic, mechanism and economic analysis, Ecol. Eng. **91** (2016) 317.
doi: https://doi.org/10.1016/j.ecoleng.2016.03.015
48. *Yu, H., Liu, Y., Shu, X., Fang, H., Sun, X., Pan, Y., Ma, L.,* Equilibrium, kinetic and thermodynamic studies on the adsorption of atrazine in soils of the water fluctuation zone in the Three-Gorges Reservoir, Environ. Sci. Eur. **32** (2020) 1.
doi: https://doi.org/10.1186/s12302-020-00303-y
49. *Guo, N., Lv, X., Li, Q., Ren, T., Song, H., Yang, Q.,* Removal of hexavalent chromium from aqueous solution by mesoporous α-FeOOH nanoparticles: Performance and mechanism, Microporous Mesoporous Mater. **299** (2020) 110101.
doi: https://doi.org/10.1016/j.micromeso.2020.110101
50. *Saha, P., Chowdhury, S.,* Insight Into Adsorption Thermodynamics. Vol. 1, IntechOpen, London, 2011, pp 278.
doi: https://doi.org/10.5772/13474
51. *Bombuwala Dewage, N., Liyanage, A. S., Smith, Q., Pittman, C. U., Perez, F., Hassan, E. B., Mohan, D., Mlsna, T.,* Fast aniline and nitrobenzene remediation from water on magnetized and nonmagnetized Douglas fir biochar, Chemosphere **225** (2019) 943.
doi: https://doi.org/10.1016/j.chemosphere.2019.03.050
52. *Wang, Z., Yu, J., Zhang, L., Zhou, Y., Yang, Y., Jin, Y.,* Cellulose laurate ester aerogel as a novel absorbing material for removing pollutants from organic wastewater, Cellulose **24** (2017) 5069.
doi: https://doi.org/10.1007/s10570-017-1489-1
53. *Wei, W., Sun, R., Jin, Z., Cui, J., Wei, Z.,* Hydroxyapatite-gelatin nanocomposite as a novel adsorbent for nitrobenzene removal from aqueous solution, Appl. Surf. Sci. **292** (2014) 1020.
doi: https://doi.org/10.1016/j.apsusc.2013.12.127
54. *Bougdah, N., Bousba, S., Belhocine, Y., Messikh, N.,* Application of multilayer perceptron network and random forest models for modelling the adsorption of chlorobenzene on a modified bentonite by intercalation with hexadecyltrimethyl ammonium (HDTMA), React. Kinet. Mech. Catal. **135** (2022) 247.
doi: https://doi.org/10.1007/s11144-021-02121-6

55. *Wang, F., Ma, Y.,* MPC-973: A low-cost and effective adsorbent for the removal of nitrobenzene from aqueous solutions, Mater. Chem. Phys. **208** (2018) 157.
doi: https://doi.org/10.1016/j.matchemphys.2018.01.049
56. *Pasti, L., Rodeghero, E., Beltrami, G., Ardit, M., Sarti, E., Chenet, T., Stevanin, C., Martucci, A.,* Insights into adsorption of chlorobenzene in high silica MFI and FAU zeolites gained from chromatographic and diffractometric techniques, Minerals **8** (2018) 80.
doi: https://doi.org/10.3390/min8030080
57. *Wang, D., Shan, H., Sun, X., Zhang, H., Wu, Y.,* Removal of nitrobenzene from aqueous solution by adsorption onto carbonized sugarcane bagasse, Adsorpt. Sci. Technol. **36** (2018) 1366.
doi: https://doi.org/10.1177/0263617418771
58. *Li, X., Zhang, X., Xu, Y., Yu, P.,* Removal of nitrobenzene from aqueous solution by using modified magnetic diatomite, Sep. Purif. Technol. **242** (2020) 116792.
doi: https://doi.org/10.1016/j.seppur.2020.116792
59. *Tubić, A., Lončarski, M., Apostolović, T., Kragulj Isakovski, M., Tričković, J., Molnar Jazić, J., Agbaba, J.,* Adsorption mechanisms of chlorobenzenes and trifluralin on primary polyethylene microplastics in the aquatic environment, Environ. Sci. Pollut. Res. **28** (2021) 59416.
doi: https://doi.org/10.1007/s11356-020-11875-w
60. *Li, G., Wang, B., Xu, W. Q., Li, Y., Han, Y., Sun, Q.,* Enhanced nitrobenzene adsorption in aqueous solution by surface-silanized fly-Ash-Derived SBA-15, ACS Earth Sp. Chem. **2** (2018) 246.
doi: https://doi.org/10.1021/acsearthspacechem.7b00127
61. *Wu, Y., Qi, H., Li, B., Zhanhua, H., Li, W., Liu, S.,* Novel hydrophobic cotton fibers adsorbent for the removal of nitrobenzene in aqueous solution, Carbohydr. Polym. **155** (2017) 294.
doi: https://doi.org/10.1016/j.carbpol.2016.08.088